JOURNAL OF MATERIALS SCIENCE 28 (1993) 1090–1096

Determination of the mechanical properties of amorphous Ni–Cr–P alloys

A. WOLFENDEN, S. K. R. KONDLAPUDI
Advanced Materials Laboratory, Mechanical Engineering Department, Texas A and M University, College Station, TX 77843, USA

The mechanical properties of Ni(80 − x) Cr(x) P(20) amorphous alloys (with x = 0–40 at % in steps of 5 at %), produced by melt spinning, have been determined. The amorphous nature of the alloys was confirmed by X-ray diffraction. Differential scanning calorimetry showed that the crystallization temperatures increased with increasing chromium content. Microhardness measurements, made on both the wheel and free sides of the as-cast ribbons, revealed the presence of a gradient in hardness through the thickness of the specimens. Dynamic Young's modulus was measured with the piezoelectric ultrasonic composite oscillator technique and tensile fracture strengths were determined by uniaxial tensile testing of selected ribbons. Correlations were developed among the various properties to gain an insight into the structure/properties relations for these materials.

1. Introduction

Over recent years, the many fundamental investigations of the mechanical and physical properties of amorphous alloys (or metallic glasses) have revealed interesting prospects for applications. Metallic glasses can be used as low-cost, high strength materials for reinforcement of concrete and plastics, for cord materials in automobile tyres and in energy storage devices such as flywheels. Amorphous alloys' low coefficients of thermal expansion and low-temperature coefficients of Young's modulus can facilitate their usage in precision instruments. By virtue of their high strength, good bendability and excellent corrosion resistance, metallic glasses make an excellent choice of material for cutting tools [1]. The magnetic properties of certain amorphous alloys can also be put to several uses.

While several authors have investigated the Ni–P amorphous alloys [2–9], the ternary Ni–Cr–P system remains one of the most promising systems. With 20 at % P, these alloys can be prepared easily in the amorphous phase [10]. Above 25 at % Cr, the Ni–Cr–P amorphous alloys become extremely corrosion resistant [11]. To realize fully the prospects for applications of these metallic glasses, their mechanical properties must be determined. In this paper, we report the determination of the mechanical properties (microhardness, tensile fracture strength and dynamic Young's modulus), density and crystallization temperature of Ni(80 − x)Cr(x)P(20) alloys with x = 0–40 at % in increments of 5 at %, prepared by melt spinning. The correlations developed among the various properties are examined so as to gain further insight into the structure of the amorphous Ni–Cr–P system.

2. Experimental procedure

The starting materials used for the preparation of the Ni–Cr–P alloys were CrP powder 99.5% pure, Cr powder 99.95% pure, Ni_2P powder 99.5% pure and Ni powder 99.9% pure. From these starting materials, Ni_4P and Cr_4P powders were prepared and pressed into pellets at room temperature under a pressure of 35 MPa. These pellets were melted in an arc furnace in an argon atmosphere to obtain Ni_4P and Cr_4P ingots. From these ingots, the Ni(80 − x)Cr(x)P(20) alloys (with x = 0–40 in steps of 5 at %) were prepared by arc melting. An alloy with composition Ni78Cr2P20 was also prepared. Chemical analysis of two of these alloys, for which maximum weight losses were observed during the arc melting, confirmed that the concentrations of the alloys prepared in this way were produced to within 0.5 at %.

For the melt spinning, approximately 1 g of the alloy at a time was melted under argon in a quartz crucible fitted with a 0.8 mm diameter circular orifice. The furnace was a radio frequency generator with a suitable coil. The crucible-wheel spacing was 2 mm and the molten alloy was ejected at a pressure of 84–112 kPa on to the copper wheel rotating at 26–30 ms^{-1}. The wheel side of the ribbon thus produced was observed to be dull compared to the free side of the ribbon. Typical widths and thicknesses of the ribbons were 2 and 0.015 mm, respectively.

The Archimedes method was used to measure the mass density of the melt-spun ribbons on a Cahn microbalance of sensitivity 1 μg. The reference liquid was toluene with a density of 0.8669 $Mg\,m^{-3}$ at 296 K. Five measurements were taken for each composition of the alloy and the mean density was recorded.

The amorphous nature of the melt-spun alloys was confirmed by X-ray diffraction using the θ–2θ geometry. The X-ray source was CuK_{α_1}, with a voltage of 50 kV and a current of 180 mA.

The differential scanning calorimetry (DSC) was carried out with a Perkin–Elmer DSC 1500 on specimens of 2–8 mg. The heating rate was 10 K min^{-1}.

A Buehler microhardness tester was used to determine the Vickers hardness number (VHN) of the melt-spun ribbons. The load used was 300 g. Ten indentations each were made on both the wheel side and the free side of the ribbons, and the average values of the VHN were recorded.

The dynamic Young's modulus of the melt-spun ribbons was measured with the piezoelectric ultrasonic composite oscillator technique (PUCOT) [12], operating at 40 kHz. During the tests the strain amplitude in the specimens was in the range 4×10^{-8}–3×10^{-6}.

Uniaxial tensile tests on the ribbons were performed on an Instron tester. The edges of the specimens were polished so as to produce ribbons of uniform width. From measurements of the mass, length and width of each specimen, the thickness could be calculated. The tensile specimens were typically 100 mm long and 1.5 mm wide. Each ribbon was sandwiched at both ends between two plexiglass plates of dimensions 37.5 mm × 25 mm × 4.4 mm and sealed with Epoxy resin and hardener. The effective gauge length of the specimens was 25 mm. During the tensile tests the crosshead speed was 0.025 mm s^{-1}. The tests were repeated three times for each alloy composition, and the mean values of tensile fracture stress were recorded.

3. Results and discussion

3.1. Density

The density measurements varied in the range 7.04–7.84 Mg m^{-3}, with an experimental error of ± 1% and an average standard deviation of 0.1 Mg m^{-3}. The values of density are listed in Table I. A specimen of Ni_4P was crystallized by annealing it at 673 K for 30 min in argon. The density of the crystallized specimen was 7.91 Mg m^{-3}, amounting to an increase of 1.2% in the density upon crystallization. Such a small increase in density suggests that the theory of dense random packing of hard spheres cannot explain completely the structure of amorphous alloys, because it predicts a density for the amorphous alloy 14.8% lower than that of the corresponding close-packed crystalline alloy. Logan and Ashby [5] proposed that the replacement of hard spheres by the same distribution of softer ones and filling of the Bernal holes in the dense random packing by the metalloid can explain the similarity in the densities of the crystalline and amorphous phases.

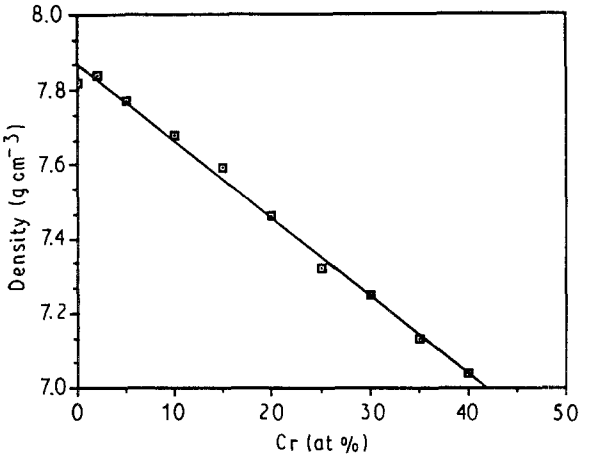

Figure 1 Mass density as a function of chromium content for Ni–Cr–P amorphous alloys.

The variation of the density as a function of chromium content is shown in Fig. 1. The density decreases as the chromium content increases, which is expected because the atomic mass of chromium is slightly lower than that of nickel. The variation of density, ρ, with chromium content, x, is described by a first order curve, with the coefficient of determination (COD) (R^2) of 0.993

$$\rho = 7.867 - 0.020\,736\,(x)\ \text{Mg m}^{-3} \qquad (1)$$

3.2. DSC

A typical DSC scan for a specimen is shown in Fig. 2. Crystallization is marked by the large exothermic peak on the plot of heat flow versus temperature. A summary of the onset and crystallization temperatures is presented in Table II. These are in close agreement with the values reported by Rhie *et al.* [10]. The variations in onset and crystallization temperatures as a function of chromium content are given in Fig. 3. The variations are linear with values of COD of 0.959 and 0.964 for the peak and onset temperatures, respectively. Thus the crystallization temperature increases linearly with chromium content.

TABLE I Density data for the Ni–Cr–P amorphous alloys

Alloy	Average density (Mg m^{-3})
Ni80 P20	7.82
Ni78 Cr2 P20	7.84
Ni75 Cr5 P20	7.77
Ni70 Cr10 P20	7.68
Ni65 Cr15 P20	7.59
Ni60 Cr20 P20	7.46
Ni55 Cr25 P20	7.32
Ni50 Cr30 P20	7.25
Ni45 Cr35 P20	7.13
Ni40 Cr40 P20	7.04

TABLE II Crystallization temperature data for the Ni–Cr–P amorphous alloys

Alloy	Onset temperature (K)	Peak temperature (K)
Ni80 P20	627.3	646.3
Ni75 Cr5 P20	654.7	661.7
Ni70 Cr10 P20	682.6	695.8
Ni60 Cr20 P20	694.7	701.8
Ni50 Cr30 P20	722.4	728.8
Ni40 Cr40 P20	753.7	762.3

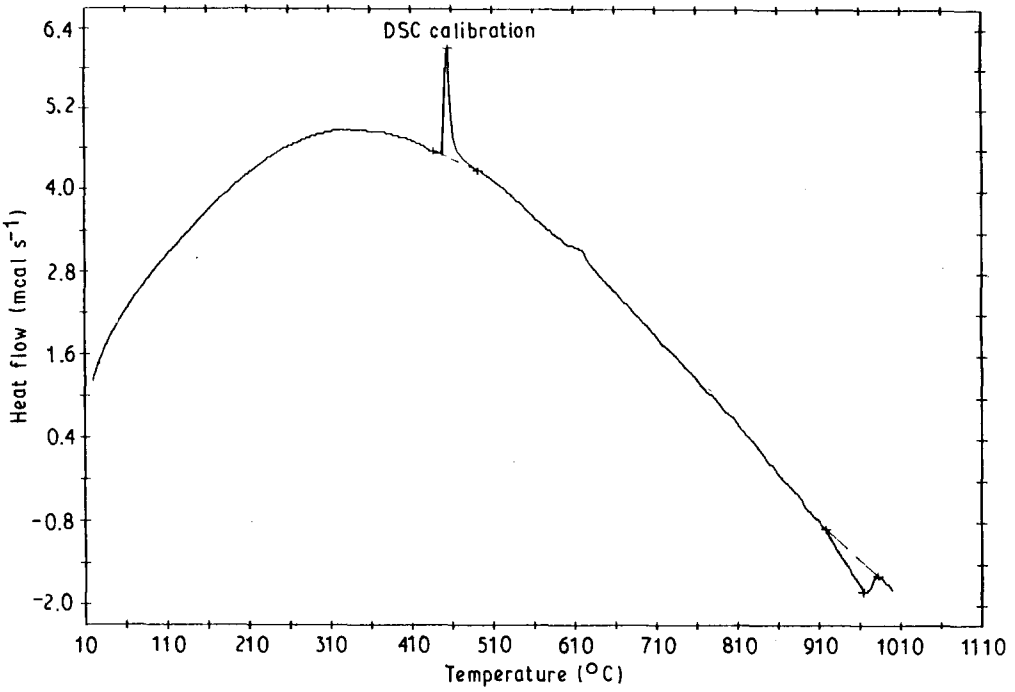

Figure 2 DSC scan for Ni50Cr30P20 amorphous alloy.

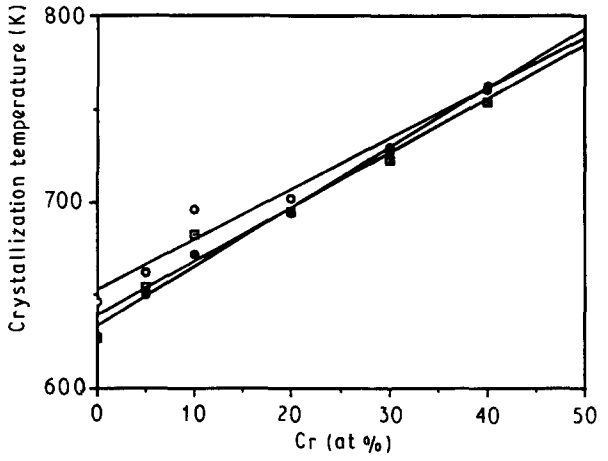

Figure 3 Crystallization temperatures as a function of chromium content for Ni–Cr–P amorphous alloys. (□) Onset temperatures, (○) peak temperatures, (●) data from Rhie *et al.* [10].

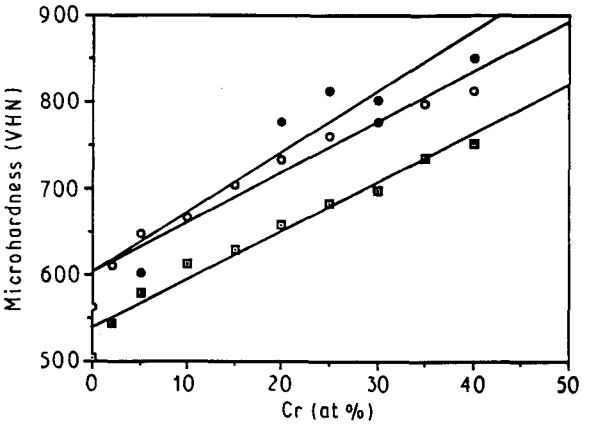

Figure 4 Microhardness as a function of chromium content for Ni–Cr–P amorphous alloys. (□) Wheel side, (○) free side, (●) data from Rhie *et al.* [10].

3.3. Microhardness

The microhardness measurements were performed on the wheel side and free side of the as-cast ribbons. The results indicate that the VHN varied from 505–751 for the wheel side of the specimens and from 562–812 for the free side, when the chromium content varied from 0–40 at %. The microhardness data are summarized in Table III. The experimental uncertainty was ± 5% for the hardness measurements and the mean standard deviation was 60 VHN. The present results are in agreement with those of Naka *et al.* [13], who predicted a loss of strength when elements to the right of iron in the Periodic Table (nickel) are substituted for iron, and an increase in strength on substitution by elements with lower atomic number (chromium). The linear variation in VHN with chromium content is seen in Fig. 4. The values of COD are 0.951 and 0.966 for the free side and wheel side of the specimens, respectively. The increase in hardness with chromium content can be attributed to the good correlation between the microhardness and the average electron concentration per metal atom, higher hardness corresponding to lower d-electron concentrations.

TABLE III Microhardness data (Vickers hardness number) for the Ni–Cr–P amorphous alloys

Alloy	Average microhardness (VHN)	
	Wheel side	Free side
Ni80 P20	505	562
Ni78 Cr2 P20	544	611
Ni75 Cr5 P20	580	647
Ni70 Cr10 P20	613	666
Ni65 Cr15 P20	629	704
Ni60 Cr20 P20	659	734
Ni55 Cr25 P20	683	759
Ni50 Cr30 P20	697	776
Ni45 Cr35 P20	736	799
Ni40 Cr40 P20	751	812

From the microhardness measurements, it is observed that the free side of the specimens is 10%–12% harder than the wheel side. This indicates that the microhardness is not uniform throughout the thickness of the specimens, with the free side being more resistant to penetration. This difference in microhardness can be attributed to the melt-spinning technique. The lower cooling rate for the free side of the specimen leads to greater solidification time, thereby facilitating the development of a higher degree of short-range order. This higher degree of short-range order on the free side accounts for a lower degree of free volume and hence higher hardness.

3.4. Tensile fracture strength

The uniaxial tensile strengths of the Ni–Cr–P amorphous alloys varied between 1960 and 2671 MPa when the chromium content varied from 0–40 at %. For each specimen, the load increased essentially linearly to fracture. The experimental error was approximately ± 5% and the average standard deviation for the tensile fracture strength data was 160 MPa. The tensile data are summarized in Table IV.

The tensile fracture strengths of the Ni–Cr–P metallic glasses are higher than those of conventional high-strength steels. The high strengths of these alloys are in sharp contrast to those of common non-metallic glasses, which fail by brittle fracture with no apparent plastic deformation, at low stress levels. Although not much ductility is observed, the materials did not fracture in a completely brittle fashion. The fracture of these metallic glasses was ductile in the sense that the fracture process was the result of large local plastic strain. The flow process is inhomogeneous, as the strain is concentrated in a few, very thin shear bands, within which the plastic strain is very large. This microscopic ductility is probably responsible for the high strengths observed, because it allows stress relief at concentrators that otherwise would cause brittle failure at much lower stresses. Non-metallic glasses do not exhibit this ductility and hence fail in a brittle manner.

The tensile fracture strength of the Ni–Cr–P alloys increased linearly with chromium content as shown in Fig. 5. The fitted curve has a COD of 0.987 and the equation relating fracture strength, σ_f, to chromium content, x, is

$$\sigma_f = 1995 + 17.104\,(x)\ \text{MPa} \qquad (2)$$

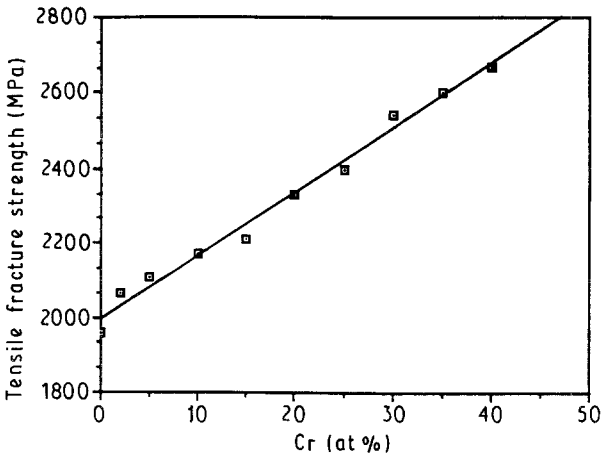

Figure 5 Tensile fracture strength as a function of chromium content for Ni–Cr–P amorphous alloys.

3.5. Dynamic Young's modulus

The values of dynamic Young's modulus obtained with the PUCOT varied between 105 and 135 GPa for the alloys studied. The data are shown in Table V with each result being the average for five specimens. The average standard deviation for the Young's modulus was 4 GPa. This reflects variation from specimen to specimen rather than the lack of precision of the technique. The elastic modulus was found to vary with thickness of the specimen, because the higher specimen thicknesses correspond to lower solidification rates, resulting in increased structural ordering, and hence increases in stiffness [14].

The value of Young's modulus reported for Ni_4P [5] is 30% higher than that found here for amorphous Ni_4P specimens. This can be rationalized by noting that in amorphous materials the atoms do not lie at centres of symmetry but move in a complicated way under elastic stresses, thereby resulting in a lower stiffness compared to that for a crystalline material. Young's modulus is dominated by structural and compositional short-range orderings due to the strong interaction between metal and metalloid atoms which hinder internal displacements. Electronic, magnetic

TABLE IV Tensile fracture strength data for the Ni–Cr–P amorphous alloys

Alloy	Tensile fracture strength (MPa)
Ni80 P20	1960
Ni78 Cr2 P20	2065
Ni75 Cr5 P20	2107
Ni70 Cr10 P20	2173
Ni65 Cr15 P20	2212
Ni60 Cr20 P20	2331
Ni55 Cr25 P20	2398
Ni50 Cr30 P20	2545
Ni45 Cr35 P20	2602
Ni40 Cr40 P20	2671

TABLE V Young's modulus data for the Ni–Cr–P amorphous alloys

Alloy	Young's modulus (GPa)
Ni80 P20	105
Ni78 Cr2 P20	109
Ni75 Cr5 P20	111
Ni70 Cr10 P20	115
Ni65 Cr15 P20	117
Ni60 Cr20 P20	121
Ni55 Cr25 P20	126
Ni50 Cr30 P20	131
Ni45 Cr35 P20	133
Ni40 Cr40 P20	136

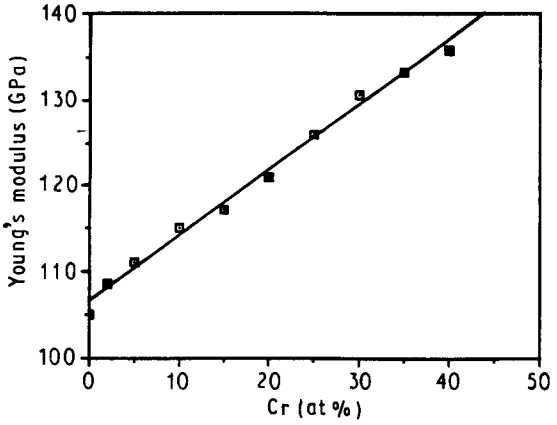

Figure 6 Young's modulus as a function of chromium content for Ni–Cr–P amorphous alloys.

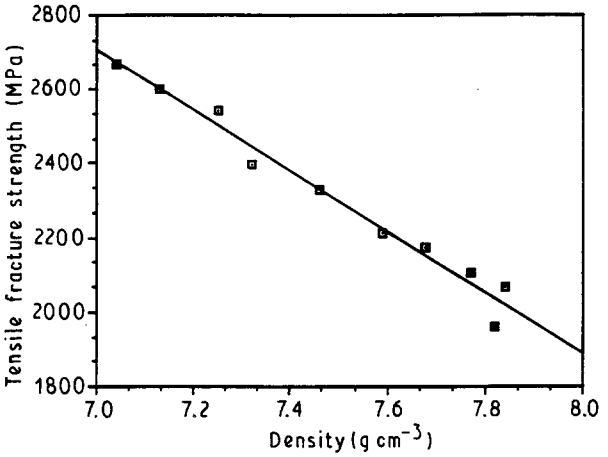

Figure 8 The correlation between tensile fracture strength and mass density for Ni–Cr–P amorphous alloys.

and low-temperature heat capacity data tend to confirm that electrons transfer from the metalloid (P) and fill the d-shells of the transition metals in Ni–Cr–P alloys [7]. By filling the d-shells of the transition metals, the conduction electrons in these metallic glasses behave like those in noble metals, thereby resulting in lower elastic modulus.

Fig. 6 shows the linear variation of dynamic Young's modulus, E, with chromium content, x. The fitted curve is

$$E = 106.55 + 0.75995(x) \text{ GPa} \quad (3)$$

with a value of COD of 0.992. This increase in Young's modulus with increasing chromium content can be associated with the lowering of the d-electron concentration with increase of chromium.

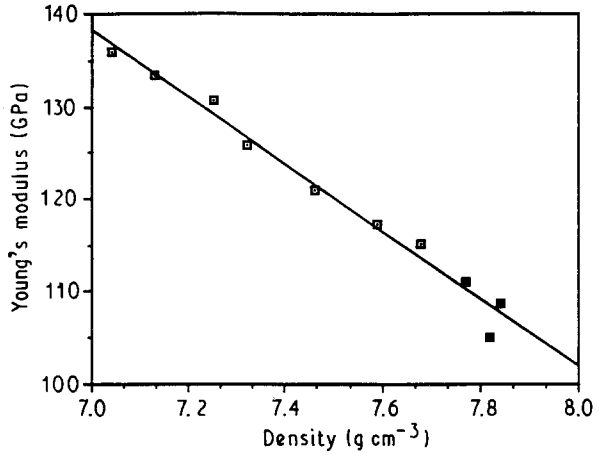

Figure 9 The correlation between Young's modulus and mass density for Ni–Cr–P amorphous alloys.

3.6. Correlations

From an examination of the results mentioned above, several correlations among the physical and mechanical properties of Ni–Cr–P melt-spun alloys emerge. The correlation between microhardness and density is shown in Fig. 7. The density and microhardness are inversely related. Similar trends are noted for σ_f–ρ and E–ρ in Figs 8 and 9, respectively. Such inverse trends observed for microhardness, elastic modulus and tensile fracture strength versus density indicate that the flow properties of these metallic glasses are determined by factors other than density. Because E/ρ is equal to the square of the longitudinal velocity of sound, the linear curve (i.e. $dE/d\rho$ = constant) in Fig. 9 confirms that the velocity of sound (i.e. $(E/\rho)^{0.5}$) in Ni–Cr–P alloys is proportional to $(\rho)^{-0.5}$, as expected. Thus, for the alloys the values of the velocity of sound lie in the range 3.66–4.40 km s^{-1}.

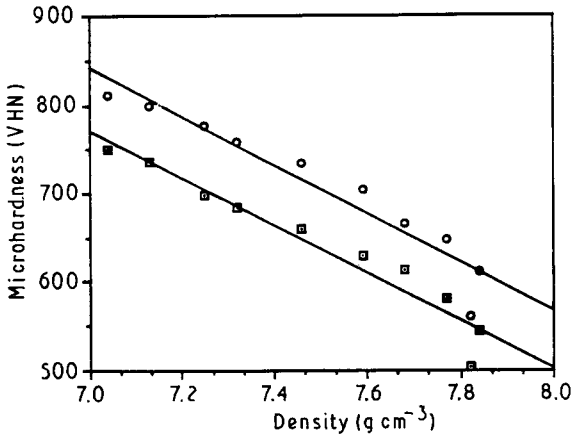

Figure 7 The correlation between microhardness and mass density for Ni–Cr–P amorphous alloys. (□) Wheel side, (○) free side.

Microhardness and crystallization temperature for the Ni–Cr–P alloys investigated indicate a similar dependence on chromium content. The correlations between the peak and onset temperatures and VHN arise from the strong correlation between mechanical and thermal behaviour and average electron concentration.

The correlation between Young's modulus and microhardness is given in Fig. 10. It is evident that the compositional dependence of E is similar to that of VHN. The first-order curves chosen for describing this behaviour have COD values of 0.976 and 0.964 for the wheel and free sides, respectively. The ratios of E/VHN for the alloys studied are listed in Table VI. These values vary between 19.05 and 17.07 when the chromium content varies between 0 and 40 at %. This indicates that the alloys with higher chromium content are stronger both on a relative as well as an absolute basis.

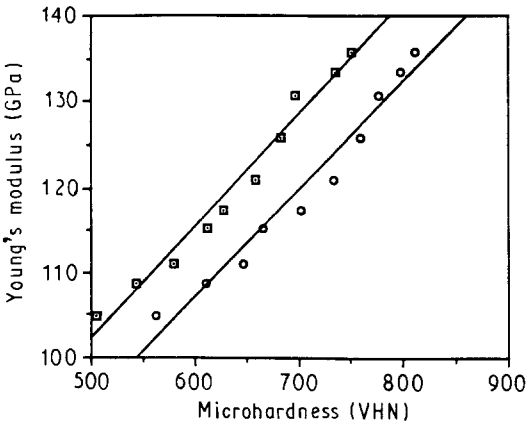

Figure 10 The correlation between microhardness and Young's modulus for Ni–Cr–P amorphous alloys. (□) Wheel side, (○) free side.

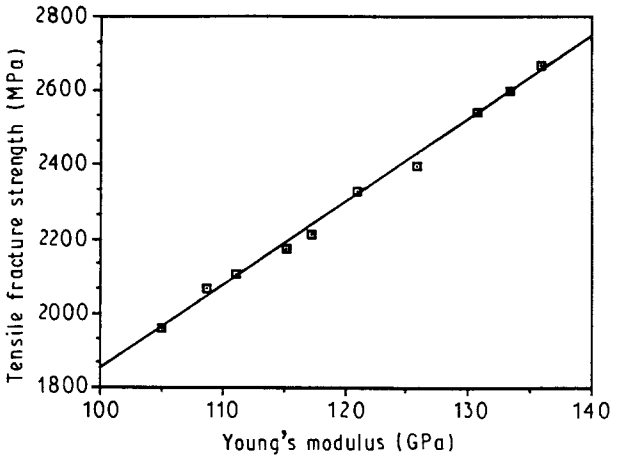

Figure 11 The correlation between Young's modulus and tensile fracture strength for Ni–Cr–P amorphous alloys.

There is a strong correlation between the tensile fracture strength and Young's modulus as shown in Fig. 11. This correlation is fitted with a linear curve of COD 0.994. Thus, increasing the stiffness of the alloy increases its fracture strength. The variations in E and σ_f with alloy composition are not due to a difference in the flow mechanism but due to a change in the short-range ordering.

For the Ni–Cr–P alloys the Young's modulus expressed as a fraction of the strength (E/σ_f) yields values around 50. In Table VI the values of E/σ_f are seen to vary between 53.56 and 50.87 for chromium

TABLE VI Hardness, tensile fracture strength and Young's modulus correlation data for the Ni–Cr–P amorphous alloys

Alloy	E/VHN[a]	E/σ_f	VHN[a]/ρ_f
Ni80 P20	19.05	53.56	2.81
Ni78 Cr2 P20	18.14	52.63	2.90
Ni75 Cr5 P20	17.49	52.70	3.01
Ni70 Cr10 P20	17.63	53.01	3.01
Ni65 Cr15 P20	16.99	53.02	3.12
Ni60 Cr20 P20	16.81	51.88	3.09
Ni55 Cr25 P20	16.90	52.48	3.11
Ni50 Cr30 P20	17.16	51.33	2.99
Ni45 Cr35 P20	17.03	51.28	3.01
Ni40 Cr40 P20	17.07	50.87	2.98

[a] VHN values have been converted to Pa.

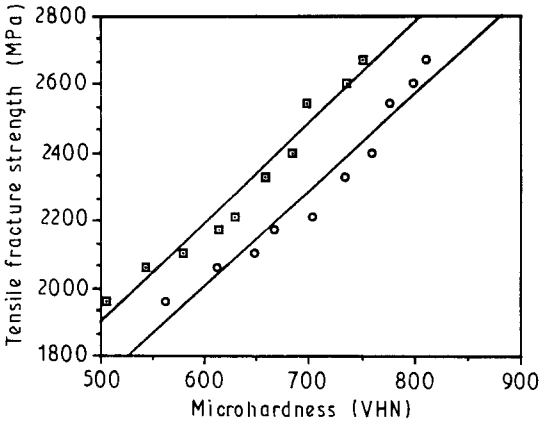

Figure 12 The correlation between microhardness and tensile fracture strength for Ni–Cr–P amorphous alloys. (○) Wheel side (□) free side.

contents in the range 0–40 at %. This is again indicative of the fact that the Ni–Cr–P alloys become stronger on a relative as well as an absolute scale with increase in the chromium content. It is interesting to compare the high values of E/σ_f for these metallic glasses with the equivalent values of 15 and 30 for iron and silicon carbide whiskers, respectively. However, the strength of whiskers is size dependent. It falls off rapidly with increasing thickness and the strength is not retained in the bulk. In contrast to the behaviour of whiskers, metallic glass specimens do not suffer much degradation in strength with increasing thickness. The theoretical strengths of these metallic glasses based on the shear modulus are of the order of 3500 MPa. Hence, the strength values of the metallic glasses approach their theoretical strengths [5]. Moreover, the values of σ_f/E are of the order of 0.02 which indicates that the critical or fracture strain (2%) is a governing factor.

The correlations between σ_f and VHN are fitted with first order curves with values of COD of 0.962 and 0.949 for the free and wheel sides, respectively, as shown in Fig. 12. The values of VHN/σ_f are presented in Table VI. It can be seen that the ratio is almost constant, varying from 2.81–3.11. Because metallic glasses exhibit large plastic flow with very little strain hardening, the strong correlation observed between σ_f and VHN is expected. The hardness measurements indicate higher strength because they test the smallest volume of the material. The smaller the test volume, the lower the probability is for that volume to contain a large flaw. Because the formation and completion of shear bands in a metallic glass is followed almost immediately by failure, the yield strength approaches σ_f.

4. Conclusions

From this study of the properties of melt spun Ni–Cr–P alloys, the following conclusions can be drawn.

1. The mass density of the alloys varied from 7.84–7.04 Mg m^{-3} as the chromium content varied from 0–40 at %. This decrease in density is expected as the atomic mass of chromium is slightly lower than that of nickel.

2. A small increase of 1.2% in the density of the amorphous alloys upon crystallization was observed. The amorphous structure can be explained by a dense random-packed model in which the hard spheres are replaced by the same distribution of softer ones and the Bernal polyhedral holes in the dense random packing are filled by the metalloid.

3. DSC measurements showed that the crystallization temperature increased linearly with increase in the chromium content, from 646–762 K. These values are in close agreement with those of Rhie *et al.* [10].

4. The microhardness tests showed that the VHN varied from 505–751 for the wheel side of the specimens and from 562–812 for the free side of the specimens when the chromium content was varied from 0–40 at %. The increase in hardness with chromium content can be attributed to the good correlation between the microhardness and the average electron concentration per metal atom, higher hardness corresponding to lower d-electron concentrations.

5. The microhardness values for the wheel side of the specimens were 10%–12% lower than those for the free side of the specimens. The lower degree of free volume for the free side of the ribbons is likely to be responsible for the higher values of hardness.

6. The tensile strengths of the alloys varied between 1960 and 2671 MPa when the chromium content was varied between 0 and 40 at %. The tensile fracture strengths of the Ni–Cr–P metallic glasses are higher than those of conventional high strength steels.

7. The values of Young's modulus varied between 105 and 135 GPa. The increase in Young's modulus with increase in chromium content can be associated with the lowering of the d-electron concentration with increase in chromium. The elastic modulus was found to vary with thickness of the specimens, higher thicknesses corresponding to increased structural ordering.

8. The Young's modulus for the amorphous alloys was 30% lower than that for the crystalline alloys. This agrees with the theory that atoms do not lie at centres of symmetry in a metallic glass but move in a complicated way under elastic stresses.

9. The compositional dependence of Young's modulus is similar to that of VHN. The values of E/VHN varied between 19.05 and 17.07 as the chromium content varied from 0–40 at %. This indicated that the alloys with higher chromium content are stronger both on a relative as well as an absolute basis.

10. Strong correlations exist between the tensile fracture strength and Young's modulus. The strength values of these metallic glasses approached their theoretical strength.

11. The ratio VHN/σ_f was almost a constant, being in the range 2.8–3.1. The strong correlation between the two parameters is expected because both are measures of the strength of a material.

Acknowledgements

The authors thank S. Cook, S. Cronauer, K. Rhie and T. Selzer, Texas A and M University, and M. Hyalt and T. Kacik, NASA Lewis Research Center, for assistance with some aspects of the experimental work, and D. Naugle and R. Griffin for valuable discussions. Financial support from the Texas Advanced Technology Research Program is also acknowledged.

References

1. T. R. ANANTHARAMAN, "Metallic Glasses – Production, Properties and Applications" (Transtech Publications, Switzerland, 1984) p. 8.
2. D. E. POLK and B. C. GIESSEN, in "Metallic Glasses" (eds.) J. J. Gilman and H. J. Leamy (American Society for Metals, Metals Park, OH, 1978) p. 19.
3. H. S. CHEN and K. A. JACKSON, *ibid.*, p. 78.
4. M. F. ASHBY, A. F. NELSON and R. M. A. CENTAMORE, *Scripta Metall.* **4** (1970) 715.
5. J. LOGAN and M. F. ASHBY, *Acta Metall.* **22** (1974) 1047.
6. L. A. DAVIS, R. RAY, C. P. CHOU and R. C. O'HANDLEY, *Scripta Metall.* **10** (1976) 541.
7. H. S. CHEN, J. T. KRAUSE and E. COLEMAN, *J. Non-Cryst. Solids* **18** (1975) 151.
8. T. MASUMOTO and R. MADDIN, *Mater. Sci. Engng* **19** (1975) 1.
9. W. JINGTANG, P. DEXING, S. QIHUNG and D. BINGZHE, *ibid.* **98** (1988) 535.
10. K. W. RHIE, P. RONG, D. G. NAUGLE, S. J. HARBERT, A. WOLFENDEN, A. CLEARFIELD and T. O. CALLAWAY, *J. Mater. Sci. Lett.* **7** (1988) 839.
11. R. B. GRIFFIN, A. WOLFENDEN, D. G. NAUGLE, D. L. COCKE and R. E. WHITE, in "Materials Architecture" Proceedings of the 10th Riso International Symposium on Metallurgy and Materials Science, (eds.) J. B. Blide-Sorensen, N. Hansen, D. Jnul Jensen, T. Leffers, H. Lilholt and O. B. Pedersen, p. 357.
12. A. WOLFENDEN, *Metall. Trans.* **11A** (1980) 1233.
13. N. NAKA, S. TOMIZAWA, T. MASUMOTO and T. WATANABE, "Rapidly Quenched Metals" (MIT Press, London, 1976) p. 273.
14. H. S. CHEN, J. T. KRAUSE, A. INOUE and T. MASUMOTO, *Scripta Metall.* **17** (1983) 1413.

Received 16 January
and accepted 25 June 1992